Effects of KF and RbF post deposition treatments on the growth of the CdS buffer layer on CIGS thin films - a comparative study

Tim Kodalle, Leo Choubrac, Ludovic Arzel, Rutger Schlatmann, Nicolas Barreau, Christian Kaufmann

Effects of KF and RbF post deposition treatments on the growth of the CdS buffer layer on CIGS thin films – a comparative study

Tim Kodalle*[,a,b], Léo Choubrac[b,‡], Ludovic Arzel[b], Rutger Schlatmann[a,c], Nicolas Barreau[b], and Christian A. Kaufmann[a]

[a] *PVcomB/Helmholtz-Zentrum Berlin für Materialien und Energie, Schwarzschildstr. 3, 12489 Berlin, Germany. Fax: +4930 8062 15677; Tel: +4930 8062 18139; E-mail: tim.kodalle@helmholtz-berlin.de*

[b] *Institut des Matériaux Jean Rouxel (IMN-UMR6502), Université de Nantes, CNRS, 2 Rue de la Houssinière BP32229, 44322 Nantes Cedex 3, France.*

‡ *Additional Present Adress: Department of Structure and Dynamics of Energy Materials, Helmholtz-Zentrum Berlin für Materialien und Energie, Hahn-Meitner-Platz 1, 14109 Berlin, Germany*

[c] *Hochschule für Technik und Wirtschaft Berlin, Treskowallee 8, 10318 Berlin, Germany.*

Abstract

In this contribution we are analyzing and comparing the impact of two different alkali-fluorine post deposition treatments (KF and RbF) on the growth of chemical-bath-deposited CdS buffer layers on $Cu(In,Ga)Se_2$ absorber layers for thin film solar cells. By combining Raman scattering, scanning electron microscopy, current-voltage analysis and measurements of the internal quantum efficiency we provide a comprehensive picture of this issue on the material and device level. We find that both PDTs lead to a better CdS-coverage of the surface of the CIGS, which leads to an improved junction quality at early growth stages compared to untreated devices. Furthermore the growth rate of the CdS is enhanced on KF-treated absorber layers while it is decreased on those treated with RbF (compared to the reference). This leads to a more stable behavior of RbF-treated devices after longer duration of the CdS deposition, while the KF-treated devices suffer from reduced fill factor and open circuit voltage. Furthermore we show that not only both PDTs but also the growth of the CdS lead to a reduction of the amount of the so called ordered defect compound, which is initially present at the surface of our absorber layers. This behavior indicates either the formation of Cd_{Cu}-anti-sites or of a secondary phase at the interface.

Keywords: CdS growth, CIGS solar cells, post deposition treatment, alkali fluorides, Raman scattering, ordered defect compound

1. Introduction

Since most of the latest progress in increasing the efficiency of solar cells based on $Cu(In,Ga)(Se,S)_2$ (CIGSSe) absorber layers was achieved by application of an alkali-fluoride post deposition treatment (PDT) using KF, RbF or CsF [1][2][3], a lot of recent studies are focusing on the mechanisms involved during the PDTs [4, 5, 6, 7, 8, 9, 10, 11, 12, 13, 14]. While the main effects of these PDTs are enhancement of the open-circuit voltage (V_{OC}) and fill factor (FF), it was also reported that they provide the opportunity to grow the commonly used CdS buffer layer thinner than on untreated samples without losing performance [1, 4]. Since the bandgap of CdS is rather narrow ($E_g^{CdS} = 2.4\,eV$ [15]), a thinner buffer layer leads to reduced absorption losses in the buffer layer and therefore to a gain in short-circuit current density (j_{SC}). There is one study in which the authors could show that an alkali-PDT leads to a better coverage of the $Cu(In,Ga)Se_2$ (CIGS) by the subsequently deposited CdS in early growth stages as well as to a faster growth rate of the CdS [16]. The latter result was already mentioned in another study investigating the impact of a KF-PDT on CIGS grown on flexible substrates [1]. However, to the

*Corresponding author: tim.kodalle@helmholtz-berlin.de

best of our knowledge no publication systematically investigating and comparing the effect of different PDTs on the growth of the CdS is published so far. Targeting this issue, we present a comparison of the impact of an RbF-PDT and a KF-PDT on the CdS growth. To do so, we carried out a combinatory Raman scattering and scanning electron microscopy (SEM) study to investigate the PDT-induced changes on a fundamental level. Furthermore the interplay of the typically Cu-depleted surface of CIGS absorber layers (with and without alkali-PDTs) with the subsequently deposited CdS-buffer layer is examined using Raman scattering. Finally we prepared devices with different thicknesses of the CdS layer to combine those results with the optoelectronic properties of the finished solar cells.

2. Material and Methods

In order to investigate the impact of both a KF- and an RbF-PDT on the growth of the CdS buffer layer as well as on the device performance in dependence of the thickness of the CdS, we prepared two sample sets consisting a KF-, an RbF-treated as well as an untreated reference sample each: Set 1 for the growth study and Set 2 for the device study. Therefore in total six CIGS thin film samples were deposited using a three stage co-evaporation process [17] on 1 mm thick glass substrates coated with 400 nm thick DC-sputtered molybdenum. All samples were prepared without diffusion barriers, so that Na could diffuse from the glass substrates into the films during growth. The maximum substrate temperature during the second and third stage of the process was 580°C, the integral composition as measured by X-Ray Fluorescence spectroscopy (XRF) exhibits $\frac{\chi_{\mathrm{Cu}}}{\chi_{\mathrm{Ga}}+\chi_{\mathrm{In}}} = CGI \approx 0.8$ and $\frac{\chi_{\mathrm{Ga}}}{\chi_{\mathrm{Ga}}+\chi_{\mathrm{In}}} = GGI \approx 0.35$, χ_{i} denoting the molar fraction of element i. For additional details of the CIGS deposition process the reader is referred to Ref. [18]. After the CIGS deposition samples were taken out of the system, i.e. exposed to air, and on two samples each a KF-PDT or RbF-PDT was performed respectively. The details of the KF-PDT are published in Ref. [8]. The RbF-PDT was performed at a substrate temperature of 280°C with an RbF-deposition rate of around 0.2 $\frac{\text{Å}}{\text{s}}$ in Se atmosphere. The Se-atmosphere was provided using two Se-sources aiming onto the substrate from a distance of about 50 cm. The evaporation rates of the Se-sources were set to values lower than 0.1 $\frac{\text{Å}}{\text{s}}$. The base pressure of the used system in stand-by is about 10^{-6} mbar. After depositing an approximately 10 nm thick RbF film, both the RbF and the Se-fluxes were cut off and the substrate was annealed for another 5 minutes before cooling it down. To avoid cross contamination KF- and RbF-PDTs were performed in different evaporation chambers with slightly different setups. However, since the KF-PDT and the CIGS-deposition are performed in the same chamber cross-contamination could not be ruled out entirely, and indeed, we found small traces of K in the bulk of all samples (see supporting information). Nevertheless, since the amount of K in the untreated and RbF-treated samples is about an order of magnitude lower than in the KF-treated samples and was not detected at the very surface of those samples, we assume that our results are not impaired by this cross-contamination. These K-traces could either be due to cross-contamination in the chamber or out-diffusion of K from the glass substrates.

One set of samples consisting of an untreated reference sample, a KF-PDT sample and an RbF-PDT sample was used to investigate the impact of the PDTs on a materials basis (Set 1), while the other set was used to compare their impact on the opto-electronical device properties (Set 2).

The samples of Set 1 were cut in 11 approx. 1 x 1 cm^2 sized pieces each, of which ten were dipped into an aequeuos chemical bath consisting of the followingly concentrated chemical solutions: Cd-acetate [2.6 mM], thiourea [0.1 M], and ammonia [1 M] (chemical purity of all used chemicals: $\geq$ 0.99). In order to ensure reproducible conditions a water bath was heated to 58°C and a glass beaker was dipped in it. After the temperature was stabilized, the solutions, which were prepared at room temperature, are poured into the glass beaker and the samples are added immediately. Starting after one minute one sample was taken out of the bath per minute resulting in a variation of the CBD-duration from 0 min to 10 min. To avoid cross contamination the untreated, KF-treated, and RbF-treated samples were dipped separately. The samples of Set 2 were cut in 4 pieces each, which were dipped in a similar CdS bath for 3 min, 4.5 min, 7 min, and 9 min respectively. Details of the CBD-process as well as a literature overview about the CdS growth mechanism have already been recently reported in a previous study [19]. Afterwards these samples were coated with a bi-layer of intrinsic and Al-doped ZnO, which were both deposited by RF sputtering. A Ni-Al-Ni front contact grid was subsequently deposited using a electron beam evaporation.

SEM-images were taken with a Jeol JSM-7600F microscope using a 5 kV acceleration voltage and j-V curves were

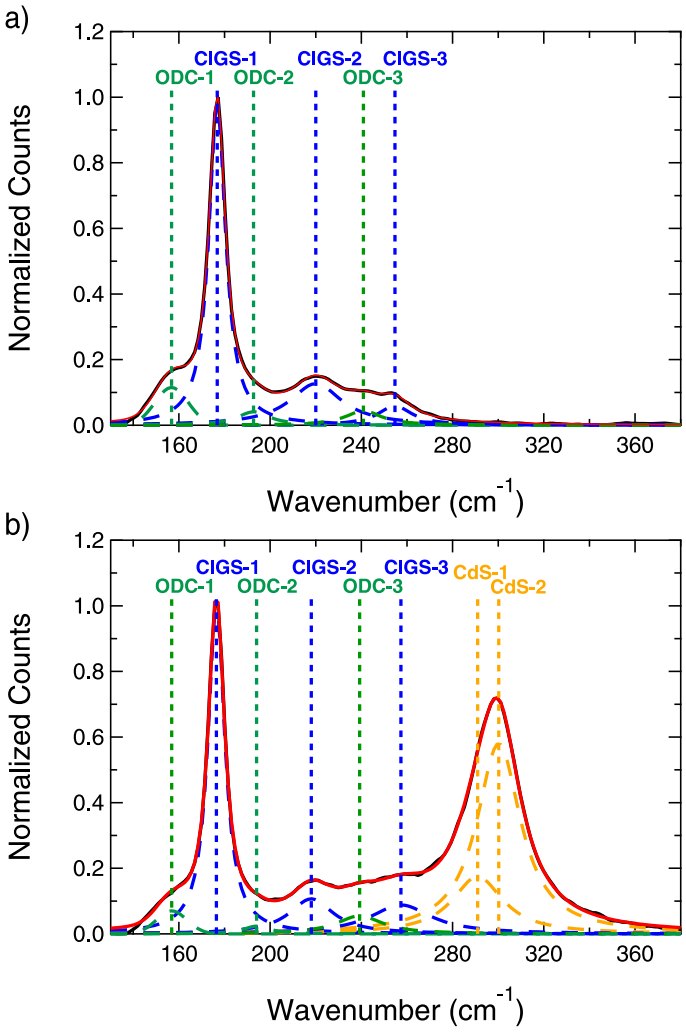

Figure 1: Examples for the fitting routine used to analyze the recorded Raman spectra. a) Spectrum after 0 min CBD showing no CdS contributions. b) Spectrum after 5 min CBD showing contributions of CIGS, ODC and CdS.

measured under AM 1.5 standard test conditions. The internal quantum efficiency (IQE) was calculated from external QE measurements performed in a self-built setup. The latter were corrected by reflection measurements in a UV-Vis spectrometer by Perkin Elmer. Raman spectra were recorded in back-scattering configuration on a Jobin-Yvon T64000 spectrometer coupled to a microscope (spot surface $5\,\mu m^2$) at 514.5 nm excitation wavelength. We recorded five spectra on different spots of each piece of Set 1 to take lateral inhomogeneities into account. Subsequently we removed the background from the recorded spectra using the software fityk [20] and fitted all spectra with a combination of 6 peaks (samples with no CdS signature visible) or 8 peaks respectively (samples with visible CdS contributions). In Figure 1 representative examples of a spectrum with (1 a)) and without CdS-contributions (Figure 1 b)) including the respective fits are shown. We attributed one peak each to the CIGS A_1 (CIGS-1) [21], and the B- and E- contributions (CIGS-2, -3), three to the respective contributions of the so called ordered defect compound (ODC-1, -2, -3), a compound with reduced Cu-content, [22] as well as two peaks to the longitudinal optical (LO) phonon scattering in the CdS (CdS-1, -2) [23]. Being aware that more Raman active modes are reported for each of these materials [21, 22, 23], we chose this fitting routine in order to maintain stable fitting conditions. All spectra were then normalized to the maximum of the CIGS A1 mode.

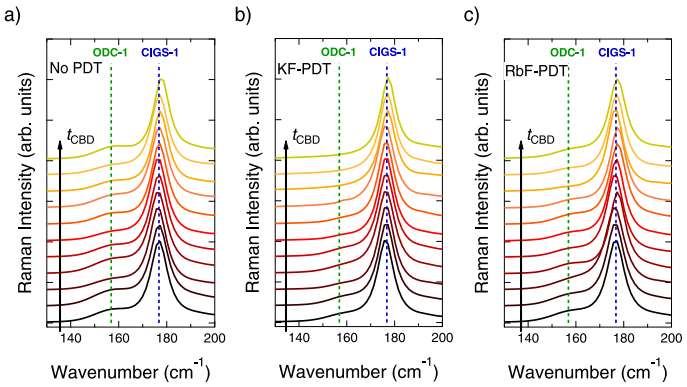

Figure 2: Examples of how the "A1-region" of the three different sample sets evolves during the CdS deposition in case of untreated CIGS (a), KF-treated CIGS (b) and RbF-treated CIGS (c). The deposition time of the CdS is indicated by t_{CBD}. The initial reduction of the ODC-feature as well as the steady vanishing of its residuals during the CBD are clearly visible.

3. Analysis of the ODC-Signature

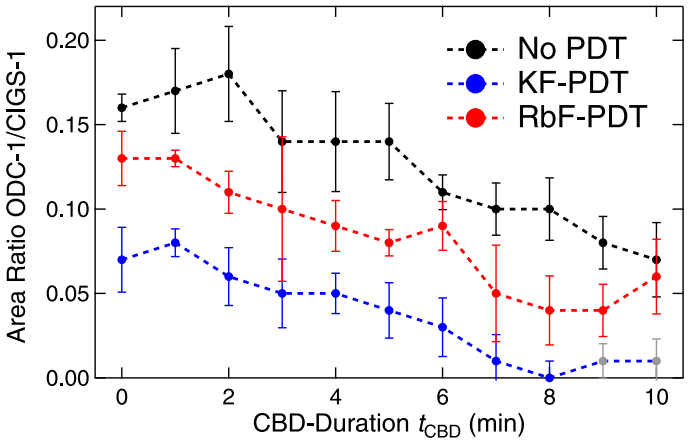

Figure 3: Evolution of the area ratio of the ODC-1 and the CIGS-1 peak for all three sets during the CdS deposition. Dashed lines are shown as guidance for the eye only. Error bars show the standard deviation calculated from the five measurements which were done on each sample.

In Figure 2 one example fit of the A1-region of the Raman spectra of each sample from Set 1 is shown. In order to analyze the impact of both PDTs as well as the CdS growth on the ODC signature, the area ratio of the ODC-1 contribution over CIGS-1 was calculated for all five measurements of each sample. The average of these five measurements is plotted versus the CdS deposition duration (t_{CBD}) in Figure 3. It is evident that both PDTs lead to a significant reduction of the ODC mode.

To quantify this reduction a linear fit of all three curves was performed. Due to the fact that there are barely any traces of the ODC-1 detectable on the KF treated samples after 8 min, we restricted the fit of this set to the range 0-8 min and did not include the points at 9 and 10 min in the fit. According to the fit results, the initial reduction due to KF is stronger pronounced (reduction of $(48 \pm 5)\,\%$, while RbF-PDT leads to a reduction of $(16 \pm 5)\,\%$ compared to the untreated reference). However, with longer CBD duration the ODC-contribution is (further) reduced in all three cases with indistinguishable rates: the slope of the linear fit is (-0.009 ± 0.001) per minute for the untreated samples and (-0.011 ± 0.001) per minute for both the KF-treated and the RbF treated ones. Note again, that Figure 3 shows the ratio of the ODC-1 and the CIGS-1 contribution, meaning that this is not an attenuation effect of CdS covering the surface of the CIGS. Moreover this is an indicator for a direct

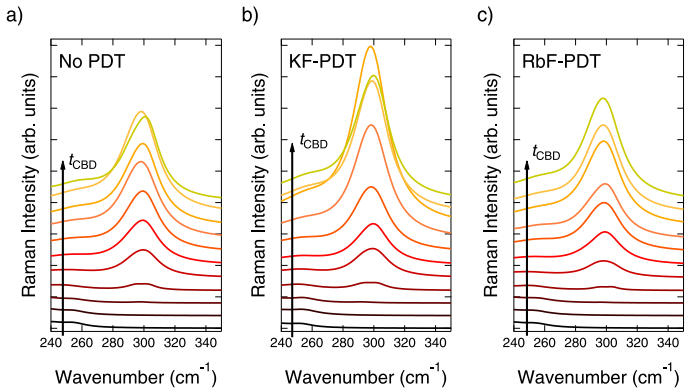

Figure 4: Raman spectra of one measurement per sample of each set. The plotted region only shows the combined contributions CdS-1 and CdS-2 - still all spectra are normalized to the respective CIGS-1 contribution. a) shows the reference set, b) the KF-treated set and c) the RbF-treated set.

consumption of the ODC phase during the CBD. Due to the different initial offsets depending on the nature of the PDT, the final values differ too. While there is no trace of the ODC left on the KF-treated samples already after 8 min CBD, there are still clear contributions detectable after 10 min CBD duration on the RbF treated and the untreated samples.

4. Impact of the PDTs on the CdS-growth

4.1. Raman and SEM study (Set 1)

In this section the impact of both PDTs on the growth morphology (analyzed by SEM) as well as on the growth dynamics (analyzed by Raman scattering) of the CdS are investigated using the samples of Set 1. Starting with the latter, Figure 4 shows the spectra in the range of the CdS LO-contributions of one example measurement on each sample. As it can be seen there are no traces of the CdS-contributions during the first 2 minutes of the CBD. Starting from 3 min the CdS-signals are steadily increasing with longer duration for all three sets. After longer duration the increase of the CdS-signals is no longer steady but becomes discontinuous. This can also be seen from the area ratio plot in Figure 5, which again includes data from all five measurements per sample: Starting from 7 min (KF-PDT) or 8 min (RbF-PDT and untreated samples) the error bars at each point increase and the overall evolution becomes unsteady. We attribute the phase of steady increase to the ion-by-ion growth of the CdS layer, while the unsteady behavior is due to the formation of CdS clusters on the surface of the CdS film [24]. Since the measurement spot of the Raman setup used is in the range of the size of these clusters (about 200 nm in diameter, not shown), these can influence the results strongly.

To investigate the impact of the different PDTs on the actual growth of the CdS layer, we separately interpolated the steady growth region using a linear function as it is shown in the inset of Figure 5. It can be seen from these fits that the growth rate k of the CdS is higher on surfaces treated with KF ($k = (0.98 \pm 0.11)\,\mathrm{min}^{-1}$) than on untreated surfaces ($k = (0.86 \pm 0.04)\,\mathrm{min}^{-1}$). On the other hand RbF-PDT ($k = (0.72 \pm 0.03)\,\mathrm{min}^{-1}$) leads to a lower growth rate compared to the one on the untreated surface. Hence it is evident that the CdS growth rate is slower on RbF-treated surfaces compared to the one on both KF-treated and untreated surfaces. However, the error bars of the growth rate on the KF-treated surface and the one of the reference overlap, but taking into account the appearance of the CdS-clusters, which can be qualitatively derived from Figures 4 and 5, it is nevertheless likely that the CdS growth is indeed accelerated by the KF-PDT.

To investigate the nature of these different growth rates, we examined the morphology of the growth at different stages using SEM. In Figure 6 we exemplary show top view images of all three samples after 3 minutes of the growth (additional images are shown in the Supplementary Information). Note that these SEM images were measured on a third sample set due to logistical difficulties. The samples of this third set, however, were treated exactly as the ones from the first set. The untreated CIGS at this early growth stage is just partly covered by a thin layer. While

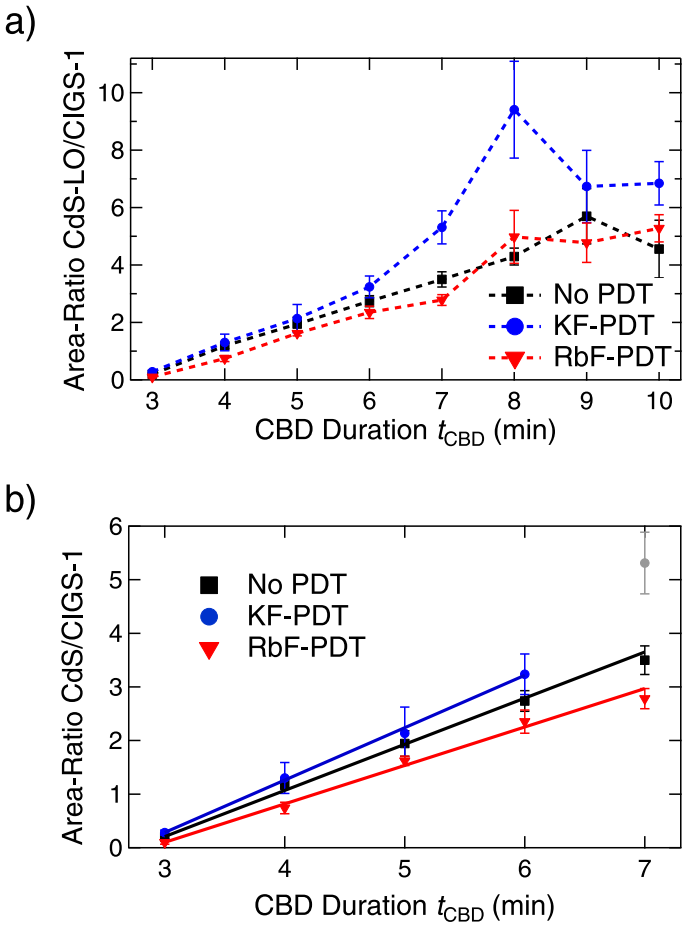

Figure 5: a) Area ratio of the combined CdS-contributions and the CIGS-1 contribution for all three sample sets in dependence of the CBD duration. Each point marks the corresponding middle value of five measurements, the error bars are given by the standard deviation. Dashed lines are guidance for the eye only.
b) Region of steady increase of the CdS/CIGS-area ratios contribution for all three sample sets. The solid lines show the result of a linear fit of the correspondingly colored measurement points.

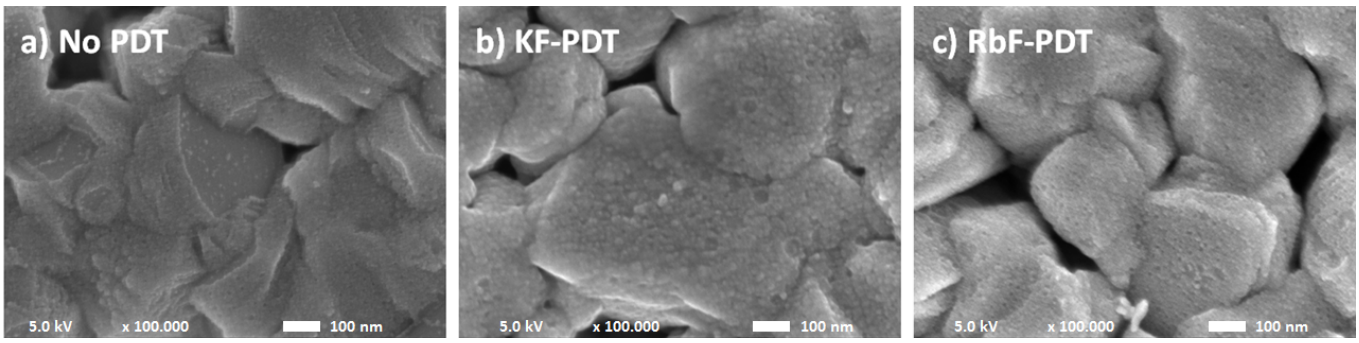

Figure 6: Top view SEM images of a reference sample (a), a KF-treated sample (b) and an RbF treated sample (c) after 3 min CBD duration.

some CIGS grains seem to be fully covered by this thin layer, others appear to be still completely blank. Both the KF- and RbF-treated surfaces appear much better covered by the CdS. There are no blank CIGS grains visible on either sample even at this early stage of the growth - so both surfaces are already completely covered by a thin film. The fact that there is already a film deposited on the CIGS after 2 and 3 min (cf. Supporting Information), but no to little CdS detectable via Raman scattering is not contradictory. It was already shown in literature [25, 19] that in the very early stages of the CdS growth there is an "induction/coalescence" mechanism taking place consisting in the adsorption of only $Cd(OH)_2$ onto the substrate. Choubrac et al. [19] also reported the beginning of the actual CdS-growth detectable by Raman to start after about 3 min.

4.2. Study of the device parameters (Set 2)

Figure 7 shows the combined j-V-parameters of two representative cells of each sample from Set 2. The solid lines are the result of interpolating the results using third degree polynomial functions (exponential function in case of j_{SC} of the untreated samples) to provide guidance for the eye only. A Figure showing a close-up to the "high-efficiency"-region of these graphs is shown in the Supplementary Information. As one can clearly see, both PDTs result in much higher values for all four parameters after 3 min, meaning they provide a higher junction quality after very short CBD duration, e.g. with a rather thin CdS layer. With longer CBD duration V_{OC} of all three sample sets is increasing and stabilizing after 7 to 9 min. This increase is slower for the reference samples, while it shows almost the same behavior for both treated samples. However, the KF-treated samples show an overall higher V_{OC} compared to the RbF treated ones. On the other hand the FF of the KF-treated samples appears to be very sensitive to the CBD duration. While the RbF-treated samples show an overall higher FF and a steadier behavior after long PDTs, KF-PDT leads to a strong deterioration of the FF after 7 to 9 min. Again the reference samples show a much slower increase and seem to reach its maximum FF after 9 min CBD duration. While j_{SC} shows slightly lower values for KF-treated samples compared to the other two sets (compare IQE results), the efficiency mostly follows the trend of the V_{OC} and FF. The KF-PDT provides high initial values, but shows decreased η already after 7 min; RbF-PDT shows similarly high initial values but more stable values after longer CBD duration; the reference samples show much lower performance after short treatments but show the most stable behavior after longer CBDs.

To be able to analyze the behavior of j_{SC} in more detail, plots of the internal quantum efficiency (IQE) are shown in Figure 8. In all three cases (No PDT, KF-PDT and RbF-PDT) one can clearly see how the increasing absorption in the CdS layer with longer CBD duration leads to lower quantum efficiencies in the wavelength region between 400 nm and 500 nm. Furthermore it becomes obvious that this effect is stronger pronounced in case of KF-treated samples, since the IQE in this wavelength region shows the lowest values after 4.5 min, 7 min and 9 min compared to the other two sample sets. There is no clear trend visible regarding RbF treated and untreated samples: after 7 min the IQE in that range is lower for the RbF-treated sample but after 9 min it is slightly lower in case of the untreated sample.

Note that the overall lower j_{SC} of the KF-treated samples is not due to a shift of the bandgap and therefore not an effect of lateral compositional gradients.

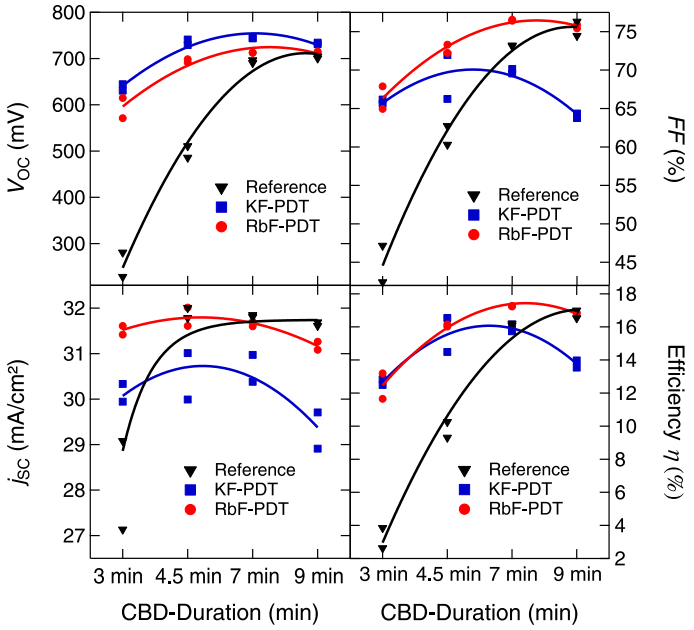

Figure 7: Electrical parameters of two cells of each sample from Set 2. The solid lines are obtained by fitting the correspondingly colored data points using a 3. degree polynomial function in all cases but the j_{SC} of the reference set, where an exponential function was chosen. These fits are used as guide to the eye only, not to interpolate the trends.

5. Discussion

5.1. Impact of the two PDTs and the CdS growth on the ODC

The fact that a KF-PDT can lead to a reduction of the ODC-signature in Raman spectra was already published before [8], while no similar behavior was reported after RbF-PDT so far. From our data, however, it becomes obvious that a comparable effect occurs in the latter case, too. We interpret these results as follows: Due to the final Cu-poor composition of the films ($CGI = 0.8$) a pronounced ODC phase is present on the untreated CIGS absorber layers. During the PDTs K and Rb atoms respectively occupy free Cu-vacancies in this surface layer reducing the amount of ODC being detectable by Raman scattering. Whether this is due to the formation of K-In-Se and Rb-In-Se phases accompanied by a Cu-diffusion deeper into the bulk as it is assumed in the literature [7, 8, 9, 11, 13, 26] or simply due to the formation of A_{Cu} anti-sites (A = K, Rb) from Cu-vacancies in the chalcopyrite lattice, which was also modeled in the literature [4], cannot directly be concluded from our data.

It was reported for both KF- and RbF-PDTs that the respective alkali-atoms are hardly incorporated into the lattice of the CIGS [27, 10, 12, 11]. Furthermore, theoretical investigations conclude that the formation of an alkali-containing non-chalcopyrite compound (as e.g. monoclinical $AInSe_2$; A = K, Rb) at the surface would be energetically favorable [28, 29]. Additionally there is experimental evidence that a non-chalcopyrite phase is forming at the surface during these PDTs [5, 7, 8, 9, 26, 11, 13], which could be even identified as $RbInSe_2$ in two separate studies [14, 30].

On the other hand some of these candidates as e.g. In_2Se_3 : K [31] and $RbInSe_2$ [29] have been proven to be Raman active, but we don't see any traces of either in the respective sample sets. However, the latter could be due to the fact that these interface phases are probably just a few nm thick [14] indicating that their Raman signal might be rather small compared to the ones of CIGS and CdS – especially since they might grow amorphous. Furthermore the most prominent Raman peaks of both phases are either overlapping with the CIGS A1 or the CdS LO-modes and would therefore not be distinguishable in our measurements.

Based on this literature data we conclude that the initial reduction of the ODC is likely to be due to the formation of alkali-In_xSe_y secondary phases. The fact that the reduction is stronger in case of the KF-PDT could be a hint for a different formation speed of the potassium containing phase or a faster in-diffusion of potassium into the CIGS

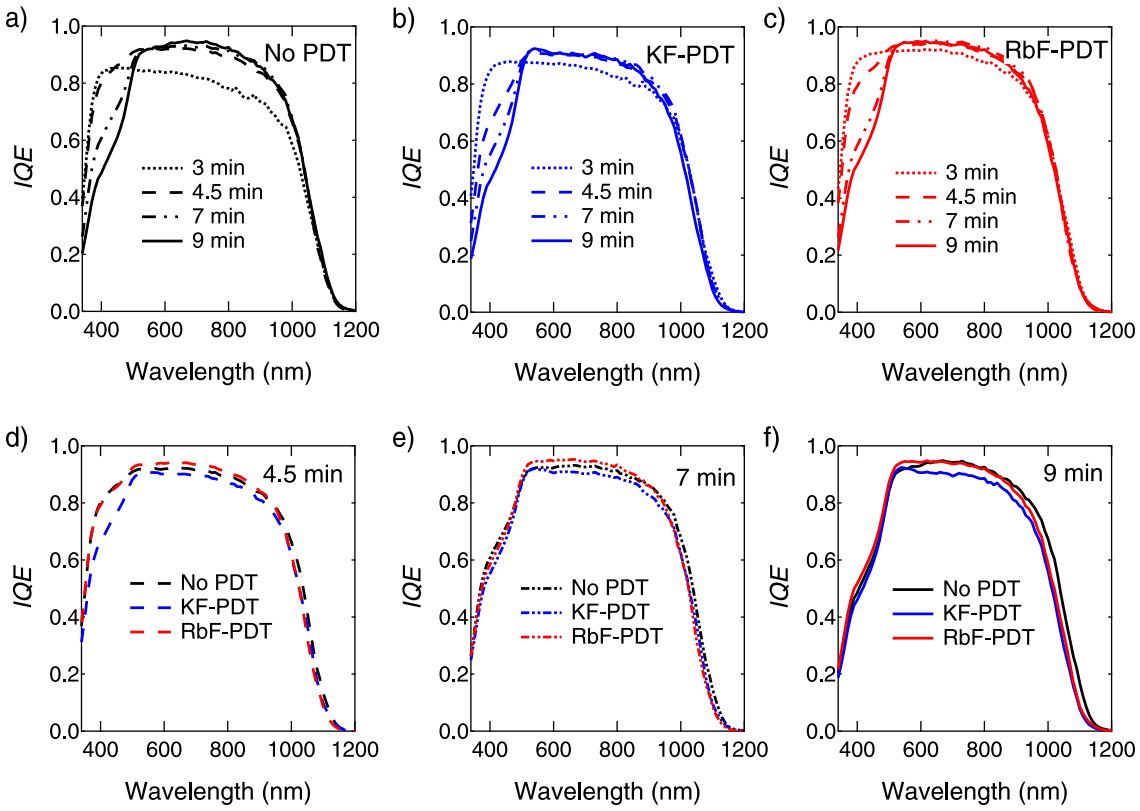

Figure 8: Internal quantum efficiencies of the best cell of each sample. IQE was obtained from measuring Reflectance and external quantum efficiency on the same cell. The image shows the results for a) the untreated reference sample, b) the KF treated sample, c) the RbF treated sample as well as combined views of all three curves of the devices with CBD-duration of d) 4.5 min, e) 7 min, and f) 9 min.

compared to the rubidium case. It can also not be ruled out that there is more K deposited during the KF-PDT than Rb during the RbF-PDT enhancing the effect in the former case, since the PDTs were done in different chambers and we are not able to quantify the amount of either in the samples. Please note that the presence and amount of the ODC are dependent on the final CGI of the samples [8] and therefore all results discussed above and in the following are likely to be dependent on the CGI as well.
The further reduction of the ODC signal during the CBD shows no dependence on the PDT performed. Generally this linear reduction could be attributed to Cd-atoms diffusing into the chalcopyrite structure creating Cd_{Cu} anti-sites from the available V_{Cu}. However, it could also be due to the formation of a mixed phase like e.g. $CdIn_2(S, Se)_4$ as it was already proposed by Barreau et al [32]. From our data it is not discernible whether this effect is amplified by the PDTs, since we cannot determine whether the amount of the ODC consumed during PDT, is further altered during the CBD growth. However, taking into account data from literature in which it was proven that the overall Cd diffusion into the CIGS is enhanced by heavy alkali-PDTs [4, 33], one can draw another conclusion from our data. Assuming that the reduction of the ODC-signal observed in our study is due to this Cd-diffusion into the absorber layer, Cd is not only occupying residual Cu-vacancies in the ODC but is additionally either occupying A_{Cu} anti-sites (A = K, Rb) in the CIGS or creating Cd_A anti-sites in the secondary phases, i.e. an ion-exchange between Cd and the alkali-atoms must go on.

5.2. Impact of the PDTs on the CdS growth

Combining the results of the Raman and the SEM study, there are two different effects of the PDTs on the subsequent growth of the CdS. The Raman study revealed that the overall growth rate is increased by the KF-PDT while it is decreased by the RbF-PDT. The SEM study on the other hand showed that both PDTs lead to a better coverage of the CIGS by CdS. It was also already shown in literature that an alkali-PDT can lead to a better coverage as well as a faster growth rate of the CdS [16]. Since the authors didn't specify the details of the PDT used, correlation with our results is impossible. However, it seems to be a general effect of the alkali-PDTs that the coverage of the CdS is enhanced. It was previously reported that the CdS growth in the early stages is strongly dependent on the orientation of the underlying CIGS grains [34] and on untreated absorber layers grains with $\langle 221 \rangle$ orientation are likely to not be covered in early growth stages. The authors explained this behavior with the lower surface energy of $\langle 221 \rangle$ oriented grains. In a subsequent contribution they showed that the growth of the CdS on these grains can be enhanced by increasing the surface energy by oxidation of the surface [35]. Due to the hydrophilic nature of alkali-salts, alkali-PDTs can lead to a stronger oxidation of the surface of the absorber layer, too [8]. Therefore the better coverage could be due to an indirect oxidation of the CIGS in between the PDTs and the CBD due to the presence of the alkali elements. Another possibility is that the orientation of the underlying CIGS grains does not play a role for the CdS growth after the PDT since all grains are covered with a monoclinic $AInSe_2$-phase. It was shown by Lincot et al. [25] that a change of the substrate can lead to significantly thicker CdS-layers under unchanged growth conditions.
The effects of the PDTs on the growth rate of the CdS are independent of the better coverage, i.e. faster on KF-treated and slower on RbF-treated surfaces. We were not able to identify a possible reason for this difference with our used methods yet.

5.3. Study of the device parameters

Taking into account the results of the j-V-measurements of corresponding solar cells, it becomes obvious that the CdS-coverage seems to be the most important factor for establishing a high-quality p-n-junction. Independent of the CdS-growth rate, both alkali-treatments lead to much higher V_{OC}, FF, and j_{SC} compared to the untreated reference at early stages of the growth. This effect could additionally be supported by the formation of the alkali-In_xSe_y layers at the surface of the CIGS as discussed above. The formation of such a high bandgap and supposedly n-type interface layer [29] may strongly reduce the interface recombination velocity, which becomes even more relevant at early growth stages of the buffer.
The higher CdS-growth rate on the KF-treated samples on the other hand induces a rather narrow process window for CBD. The maximum FF, j_{SC}, and efficiency seem to lie in the range of 4.5 to 7 min duration. 7 min CdS deposition already leads to a rather strong deterioration of the quality of the junction as well as strong absorption losses in the CdS as can be seen in the IQE. The IQE supports the results of Raman study, e.g. shows the strongest CdS-absorption for KF-treated absorber for all duration. The RbF- and untreated samples show very

similar IQE in all cases. However, after the longest CBD-duration the IQE show the same trend as the Raman study.

6. Conclusions

We compared the impact of both a KF- and an RbF-PDT on the surface of the CIGS absorber layer as well as the growth of a subsequently deposited CdS buffer layer. We could show that both PDTs are consuming the Cu-depleted surface phase of the CIGS. Based on previous studies and literature we assume that this is due to the formation of secondary alkali-In_xSe_y-phases. Furthermore we could show that the ODC is further reduced by the CdS-deposition itself. The latter could be a hint for the formation of a mixed phase like e.g. $CdIn_2(Se,S)_4$ or for enhanced Cd-diffusion into the CIGS.
Combining the results of the Raman and SEM study with the results obtained from the finished devices, one can conclude that the quality of the p-n-junction at early growth stages of the CdS is mostly determined by the lateral homogeneity of the CdS layer. Although the growth rate on the RbF treated absorber layers is lower than on the untreated ones, RbF-treated samples show much better V_{OC} and FF after short CBD-duration. The different growth rates then determine the optimal CBD duration for each sample set, since too thick buffer layers lead to a reduction of all parameters, as can be seen in case of the KF treated samples. This has to be kept in mind when analyzing the effect of different alkali-PDTs: one should make sure to individually optimize the CdS deposition for each sample set instead of comparing differently treated samples with an identical CBD-CdS.

Conflicts of interest

There are no conflicts to declare.

Acknowledgements

The authors acknowledge financial support by the German Federal Ministry for Economic Affairs and Energy in the frame of the speedCIGS project (contract number 0324095E) as well as funding from the European Union's Horizon 2020 research and innovation program under grant agreement no. 640868. Furthermore we want to thank L. Assmann for preparation of the substrates and overall technical support, J. Y. Mevellec for providing assistance at the Raman setup, N. Stephant for technical support at the SEM as well as J. Lorthioir, P. Tsoulka and P. Reyes-Figueroa for fruitful discussions.

[1] A. Chirilă, P. Reinhard, F. Pianezzi, P. Bloesch, A. R. Uhl, C. Fella, L. Kranz, D. Keller, C. Gretener, H. Hagendorfer, D. Jaeger, R. Erni, S. Nishiwaki, S. Buecheler, A. N. Tiwari, Potassium-induced surface modification of Cu(In,Ga)Se_2 thin films for high-efficiency solar cells, Nature Materials 12 (12) (2013) 1107–1111.

[2] P. Jackson, R. Wuerz, D. Hariskos, E. Lotter, W. Witte, M. Powalla, Effects of heavy alkali elements in Cu(In,Ga)Se_2 solar cells with efficiencies up to 22.6%, physica status solidi - Rapid Research Letters 10 (2016) 583–586.

[3] T. Kato, J.-L. Wu, Y. Hirai, H. Sugimoto, V. Bermudez, Record Efficiency for Thin-Film Polycrystalline Solar Cells Up to 22.9 % Achieved by Cs-Treated Cu(In,Ga)$(Se,S)_2$, IEEE Journal of Photovoltaics 9 (2018) 325–330.

[4] F. Pianezzi, P. Reinhard, A. Chirilă, B. Bissig, S. Nishiwaki, S. Buecheler, A. N. Tiwari, Unveiling the effects of post-deposition treatment with different alkaline elements on the electronic properties of CIGS thin film solar cells, Physical Chemistry Chemical Physics 16 (19) (2014) 8843.

[5] P. Pistor, D. Greiner, C. A. Kaufmann, S. Brunken, M. Gorgoi, A. Steigert, W. Calvet, I. Lauermann, R. Klenk, T. Unold, M. C. Lux-Steiner, Experimental indication for band gap widening of chalcopyrite solar cell absorbers after potassium fluoride treatment, Applied Physics Letters 105 (6) (2014) 63901–63905.

[6] P. Reinhard, B. Bissig, F. Pianezzi, H. Hagendorfer, G. Sozzi, R. Menozzi, C. Gretener, S. Nishiwaki, S. Buecheler, A. N. Tiwari, Alkali-templated surface nanopatterning of chalcogenide thin films: A novel approach toward solar cells with enhanced efficiency, Nano Letters 15 (5) (2015) 3334–3340.

[7] E. Handick, P. Reinhard, J. H. Alsmeier, L. Köhler, F. Pianezzi, S. Krause, M. Gorgoi, E. Ikenaga, N. Koch, R. G. Wilks, S. Buecheler, A. N. Tiwari, M. Bär, Potassium Postdeposition Treatment-Induced Band Gap Widening at Cu(In,Ga)Se_2 Surfaces - Reason for Performance Leap?, ACS Applied Materials and Interfaces 7 (49) (2015) 27414–27420.

[8] T. Lepetit, S. Harel, L. Arzel, G. Ouvrard, N. Barreau, KF post deposition treatment in co-evaporated Cu(In,Ga)Se_2 thin film solar cells: Beneficial or detrimental effect induced by the absorber characteristics, Progress in Photovoltaics: Research and Applications 25 (12) (2017) 1068–1076.

[9] E. Avancini, R. Carron, T. P. Weiss, C. Andres, M. Bürki, R. Figi, Y. E. Romanyuk, S. Buecheler, A. N. Tiwari, Effects of rubidium fluoride and potassium fluoride post deposition treatments on Cu(In,Ga)Se_2 thin films and solar cell performance, Chemistry of Materials 29 (22) (2017) 9695–9704.

[10] P. Schöppe, S. Schönherr, R. Wuerz, W. Wisniewski, G. Martínez-Criado, M. Ritzer, K. Ritter, C. Ronning, C. S. Schnohr, Rubidium segregation at random grain boundaries in Cu(In,Ga)Se_2 absorbers, Nano Energy 42 (2017) 307–313.

[11] S. Ishizuka, N. Taguchi, J. Nishinaga, Y. Kamikawa, S. Tanaka, H. Shibata, Group III Elemental Composition Dependence of RbF Postdeposition Treatment Effects on Cu(In,Ga)Se_2 Thin Films and Solar Cells, Journal of Physical Chemistry C 122 (7) (2018) 3809–3817.

[12] A. Vilalta-Clemente, M. Raghuwanshi, S. Duguay, C. Castro, E. Cadel, P. Pareige, P. Jackson, R. Wuerz, D. Hariskos, W. Witte, Rubidium distribution at atomic scale in high efficient Cu(In,Ga)Se_2 thin-film solar cells, Applied Physics Letters 112 (10) (2018) 103105.

[13] T. Kodalle, M. D. Heinemann, D. Greiner, H. A. Yetkin, M. Klupsch, C. Li, P. A. van Aken, I. Lauermann, R. Schlatmann, C. A. Kaufmann, Elucidating the Mechanism of an RbF Post Deposition Treatment in CIGS Thin Film Solar Cells, Solar RRL 2 (2018) 1800156.

[14] N. Taguchi, S. Tanaka, S. Ishizuka, Direct insights into $RbInSe_2$ formation at Cu(In,Ga)Se_2 thin film surface with RbF postdeposition treatment, Applied Physics Letters 113 (2018) 113903.

[15] A. I. Oliva, O. Solis-Canto, R. Castro-Rodriguez, P. Quintana, Formation of the band gap energy on CdS thin flims growth by two different techniques, Thin Solid Films 391 (2001) 28–35.

[16] T. M. Friedlmeier, P. Jackson, D. Kreikemeyer-Lorenzo, D. Hauschild, O. Kiowski, D. Hariskos, L. Weinhardt, C. Heske, M. Powalla, A Closer Look at Initial CdS Growth on High-Efficiency Cu(In,Ga)Se_2 Absorbers Using Surface-Sensitive Methods, Proceedings of the IEEE PVSC (2016) 457–461, DOI: 10.1109/PVSC.2016.7749634.

[17] I. Repins, M. A. Contreras, B. Egaas, C. DeHart, J. Scharf, C. L. Perkins, B. To, R. Noufi, 19.9%-efficient ZnO/CdS/$CuInGaSe_2$ Solar Cell with 81.2% Fill Factor, Progress in Photovoltaics: Research and Applications 16 (2008) 235–239.

[18] N. Barreau, T. Painchaud, F. Couzinie-Devy, L. Arzel, J. Kessler, Recrystallization of CIGSe layers grown by three-step processes: A model based on grain boundary migration, Acta Materialia 58 (2010) 5572–5577.

[19] L. Choubrac, G. Brammertz, N. Barreau, L. Arzel, S. Harel, M. Meuris, B. Vermang, 7.6 % CZGSe Solar Cells Thanks to Optimized CdS Chemical Bath Deposition, Phys. Status Solidi A 215 (2018) 1800043.

[20] M. Wojdyr, Fityk: a general-purpose peak fitting program, Jornal of Applied Crystallographie 43 (2010) 1126–1128.

[21] D. Papadimitriou, N. Esser, C. Xue, Structural properties of chalcopyrite thin films studied by Raman spectroscopy, Phys. Stat. Sol. (b) 242 (13) (2005) 2633–2643.

[22] C. Rincon, S. M. Wasim, G. Marin, J. M. Delgado, J. R. Huntzinger, A. Zwick, J. Galibert, Raman spectra of the ordered vacancy compounds $CuIn_3Se_5$ and $CuGa_3Se_5$, Applied Physics Letters 73 (1998) 441–443.

[23] S. Mishra, A. Ingale, U. N. Roy, A. Gupta, Study of annealing-induced changes in CdS thin films usin X-ray diffraction and Raman Spectroscopy, Thin Solid Films 516 (2007) 91–98.

[24] D. Lincot, M. Froment, H. Cachet, Advances in Electrochemical Science and Engineering, Vol. 6, Wiley-VCH, Weinheim, 1999, pages 165-235.

[25] D. Lincot, R. O. Borges, Chemical Bath Deposition of Cadmium Sulfide Thin Films. In Situ Growth and Structural Studies by Combined Quartz Crystal Microbalance and Electrochemical Impedance Techniques, J. Electrochem. Soc. 139 (1992) 1880–1889.

[26] E. Handick, P. Reinhard, R. G. Wilks, F. Pianezzi, T. Kunze, D. Kreikemeyer-Lorenzo, L. Weinhardt, M. Blum, W. Yang, M. Gorgoi, E. Ikenaga, D. Gerlach, S. Ueda, Y. Yamashita, T. Chikyow, C. Heske, S. Buecheler, A. N. Tiwari, M. Bär, Formation of a K-In-Se surface species by NaF/KF post-deposition treatment of $Cu(In,Ga)Se_2$ thin-film solar cell absorbers, ACS Applied Materials & Interfaces 9 (2017) 3581–3589.

[27] O. Cojocaru-Mirédin, P.-P. Choi, D. Abou-Ras, S. S. Schmidt, R. Caballero, D. Raabe, Characterization of Grain Boundaries in $Cu(In,Ga)Se_2$ Films Using Atom-Probe Tomography, IEEE Journal of Photovoltaics 1 (2) (2011) 207–212.

[28] M. Malitckaya, H.-P. Komsa, V. Havu, M. J. Puska, Effect of Alkali Metal Atom Doping on the $CuInSe_2$-Based Solar Cell Absorber, The Journal of Physical Chemistry C 121 (2017) 15516–15528.

[29] T. Kodalle, R. Kormath Madam Raghupathy, T. Bertram, N. Maticiuc, H. A. Yetkin, R. Gunder, R. Schlatmann, T. Kühne, C. A. Kaufmann, H. Mirhosseini, Properties of $RbInSe_2$ thin films, physica status solidi: Rapid Research Letters (2018) 1800564.

[30] N. Maticiuc, T. Kodalle, J. Lauche, R. Wenisch, T. Bertram, C. A. Kaufmann, I. Lauermann, In vacuo XPS investigation of $Cu(In,Ga)Se_2$ surface after RbF post deposition treatement, Thin Solid Films 665 (2018) 143–147.

[31] T. Lepetit, S. Harel, L. Arzel, G. Ouvrard, N. Barreau, Coevaporated KInSe 2 : A Fast Alternative to KF Post-deposition Treatment in High-Efficiency $Cu(In,Ga)Se_2$ Thin Film Solar Cells, IEEE Journal of Photovoltaics 6 (5) (2016) 1316–1320.

[32] N. Barreau, A. Frelon, T. Lepetit, E. Gautron, N. Gautier, R. Ribeiro-Andrade, N. Nicoara, S. Sadewasser, P. Zabierowski, L. Arzel, L. Choubrac, S. Harel, C. Deudon, C. Latouche, S. Jobic, M. Caldes, L. Assmann, P. Tsoulka, E. V. Pean, J. Lorthioir, F. Geschier, I. Braems, M. Moret, O. Briot, G. Ouvrard, High Efficiency Solar Cell Based on Full PVD Processed $Cu(In,Ga)Se_2/CdIn_2S_4$ Heterojunction, Solar RRL 1700140 (2017) 1–7.

[33] B. Ümsür, W. Calvet, A. Steigert, I. Lauermann, M. Gorgoi, K. Prietzel, D. Greiner, C. A. Kaufmann, T. Unold, M. Ch. Lux-Steiner, Investigation of the potassium fluoride post deposition treatment on the CIGSe/CdS interface using hard X-ray photoemission spectroscopy - a comparative study, Physical Chemistry Chemical Physics 18 (2016) 14129.

[34] W. Witte, D. Abou-Ras, D. Hariskos, Chemical bath deposition of Zn(O,S) and CdS bbuffer: Influence of $Cu(In,Ga)Se_2$ grain orientation, Applied Physics Letters 102 (051607) (2013) 1–4.

[35] W. Witte, D. Abou-Ras, D. Hariskos, Improved growth of solution-deposited thin films on polycrystalline $Cu(In,Ga)Se_2$, physica status solidi: Rapid Research Letters 10 (2016) 300–304.